JOURNAL OF GEOPHYSICAL RESEARCH, VOL. 103, NO. A8, PAGES 17,351-17,366, AUGUST 1, 1998

Broadband plasma waves observed in the polar cap boundary layer: Polar

B. T. Tsurutani,[1] G. S. Lakhina,[1,2] C. M. Ho,[1] J. K. Arballo,[1] C. Galvan,[1]
A. Boonsiriseth,[1] J. S. Pickett,[3] and D. A. Gurnett,[3] W. K. Peterson,[4]
and R. M. Thorne[5]

Abstract. Polar observations indicate the presence of intense broadband plasma waves nearly all of the time (96% occurrence frequency in this study) near the apogee of the Polar trajectory (~6-8 R_E). The region of wave activity bounds the dayside (0500 to 1800 LT) polar cap magnetic fields, and we thus call these waves polar cap boundary layer (PCBL) waves. The waves are spiky signals spanning a broad frequency range from ~10^1 to 2 x 10^4 Hz. The waves have a rough power law spectral shape. The wave magnetic component has on average a $f^{-2.7}$ frequency dependence and appears to have an upper frequency cutoff of ~(6-7) x 10^3 Hz, which is the electron cyclotron frequency. The electric component has on average a $f^{-2.2}$ frequency dependence and extends up to ~2 x 10^4 Hz. The frequency dependences of the waves and the amplitude ratios of B'/E' indicate a possible mixture of obliquely propagating electromagnetic whistler mode waves plus electrostatic waves. There are no clear intensity peaks in either the magnetic or electric spectra which can identify the plasma instability responsible for the generation of the PCBL waves. The wave character (spiky nature, frequency dependence and admixture of electromagnetic and electrostatic components) and intensity are quite similar to those of the low-latitude boundary layer (LLBL) waves detected at and inside the low-latitude dayside magnetopause. Because of the location of the PCBL waves just inside the polar cap magnetic field lines, it is natural to assume that these waves are occurring on the same magnetic field lines as the LLBL waves, but at lower altitudes. Because of the similar wave intensities at both locations and the occurrence at all local times, we rule out an ionospheric source. We also find a magnetosheath origin improbable. The most likely scenario is that the waves are locally generated by field-aligned currents or current gradients. We find a strong relationship between the presence of ionospheric and magnetosheath ions and the waves near the noon sector. These waves may thus be responsible for ion heating observed near the cusp region. Antisunward convection of these freshly accelerated oxygen ions over the polar cap during intense wave events (occurring during southward B_z events) might lead to enhanced plasma sheet O^+ population. For magnetic storm intervals this mechanism would lead to a natural delay between the main phase onset and the appearance of oxygen ions in the ring-current.

1. Introduction

Broadband plasma waves have been detected within the Earth's magnetopause low latitude boundary layer (LLBL) by the ISEE - 1 and - 2 [*Gurnett et al.*, 1979; *Tsurutani et al.*, 1981; 1989; *Anderson et al.*, 1982], GEOS [*Gendrin*, 1983; *Rezeau et al.*, 1989; *Belmont et al.*, 1995], and AMPTE [*LaBelle and Treumann*, 1988] spacecraft. Similar waves have been detected and characterized at the Jovian (magnetopause) low-latitude boundary layer [*Tsurutani et al.*, 1993, 1997]. These boundary layer waves have been demonstrated to be sufficiently intense to cause cross-field diffusion of magnetosheath plasma to form the boundary layer itself at both Earth and Jupiter [*Tsurutani and Thorne*, 1982; *Tsurutani et al.*, 1997]. If this mechanism is indeed in effect at the magnetopause, then the waves play an important role in the transfer of energy from the solar wind to the magnetosphere. This cross-field diffusion of particles, energy, and momentum would be one form of viscous interaction between the solar wind and the magnetosphere [*Axford and Hines*, 1961; *Tsurutani and Gonzalez*, 1995].

It is the purpose of this paper to report the first results of a search for waves on similar magnetic field lines as the LLBL, but using the Polar spacecraft which has an apogee of only ~9 R_E (where R_E is the Earth's radius), a much smaller distance than the magnetopause distance. In Figure 1, we show the Polar orbit, which has a high inclination and covers the noon-midnight sector. Under ordinary circumstances the Polar spacecraft does not intercept the magnetopause [*Pickett et al.*, 1997], but as shown from the diagram, the spacecraft does cross-field lines that map into the LLBL. It is the search for waves in these field regions (6 to 8 R_E from Earth) that is the focus of this paper. In this paper, we will limit our study to the dayside region.

[1]Jet Propulsion Laboratory, California Institute of Technology, Pasadena.
[2]Permanently at Indian Institute of Geomagnetism, Colaba, Bombay.
[3]The University of Iowa, Iowa City.
[4]Lockheed Space Science Laboratory, Palo Alto,California.
[5]University of California, Los Angeles, California.

Paper number 97JA03063.
0148-0227/98/97JA-03063$09.00

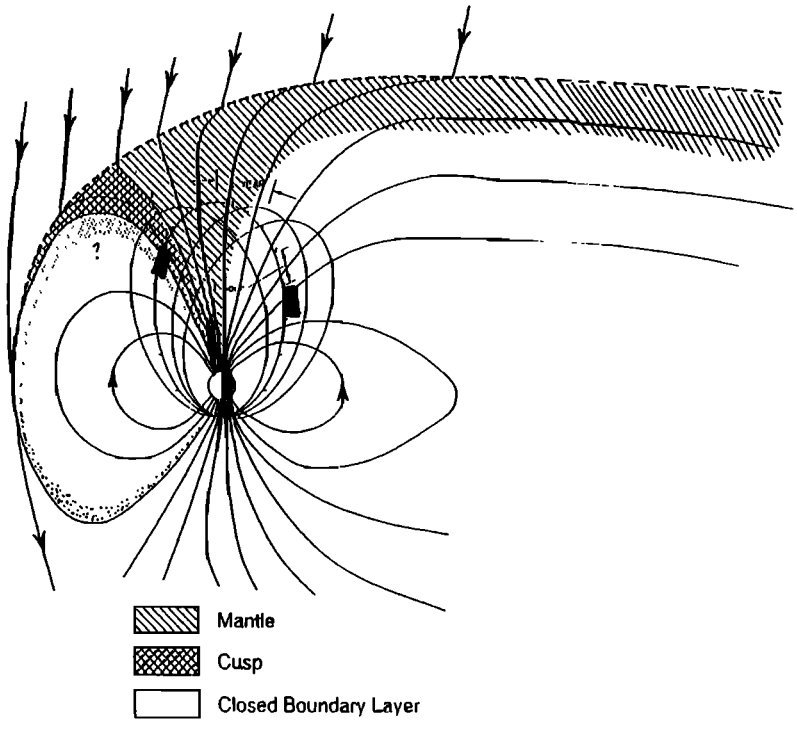

Figure 1. The Polar orbit and the region of wave detection (solid bar) in the magnetosphere. Polar has a perigee at 1.8 R_E and apogee at 9 R_E. Waves on the field lines that map into the low latitude boundary layer (LLBL) are the topic of this study.

The generation mechanism of the LLBL waves is not well understood. Some suggested mechanisms are the lower hybrid drift instability [*Gary and Eastman*, 1979; *Huba et al.*, 1981] driven essentially by the density gradients, the electron loss cone instability driven by velocity space gradients [*Kennel and Petschek*, 1966], velocity shear and drift instabilities [*Lakhina*, 1987, 1993; *Lakhina et al.*, 1993], and a magnetic shear instability [*Zhu et al.*, 1996]. The emissions are broadbanded with no obvious spectral peaks which could be used to identify particular instabilities. An electrostatic current convective instability [*Drake et al.*, 1994a] and a whistler instability [*Drake et al.*, 1994b, *Drake*, 1995] driven unstable by the gradient of the field-aligned currents with an evolution to a turbulent state, have been proposed. Through a comparison of wave intensities observed at Polar to previous measurements by ISEE, GEOS, and AMPTE and of the ratio of B'/E' to determine the wave mode(s), we hope to gain further information to help identify possible generation mechanisms/free energy sources.

We also examine the energetic (~0.1 to 10 keV or higher) ion fluxes as detected by the toroidal imaging mass-angle spectrograph (TIMAS) experiment on Polar to determine if there is a relationship between ions and the waves. A description of the TIMAS experiment is given by *Shelley et al.* [1995].

2. Method of Analysis

The Polar spacecraft and its electric dipole antennas, magnetic loop antenna, and triaxial search coil antennas are indicated in Figure 2. The three orthogonal electric dipole antennas, E_U,E_V, and E_Z, have tip-to-tip lengths of about 130, 100, and 14 m, respectively, and are used to detect the ac electric fields. Two of these electric antennas are mounted in the spin plane of the spacecraft, E_U and E_V, and one is aligned along the spin axis, E_Z. The magnetic loop antenna L, which consists of a single loop of aluminum tubing with 1.0 m^2 area, and the three orthogonal magnetic search coil antennas, B_U, B_V, and B_z, each with 20,000 turns of no. 40 wire, are mounted on the end of a 6-m rigid boom and are used to detect ac magnetic fields. The magnetic loop senses along the same direction as the electric E_U antenna. The search coil antennas, B_U, B_V, and B_Z, sense along the corresponding directions of the electric antennas, E_U, E_V, and E_Z, respectively.

We first identify wave intervals of interest by use of frequency-time spectrograms of the electric and magnetic field components of the waves which are obtained by two different types of plasma wave receivers. The sweep frequency receiver (SFR) consists of two single-sideband, phase-matched, double-conversion receivers in parallel, and are referred to as SFR-A and SFR-B (the "A" and "B" designators have no significance other than for distinguishing between the two receivers). The SFR provides good frequency resolution (about 8% at 26 Hz and 3% at 800 kHz in log-step mode) with relatively poor time resolution (one full frequency spectrum every 32 s in the log-step mode or every 64 s in the linear-step mode). The multichannel analyzer (MCA) consists of two spectrum analyzers, and are referred to as MCA-E and MCA-B (the "E" and "B" designators are used only to distinguish between the two receivers). The MCA provides good time resolution (one full frequency spectrum every 1.3 s) with relatively poor frequency resolution (4 frequency channels per decade). For more detailed information on these receivers and the antennas that are used to detect the wave signals, please refer to the plasma wave instrument (PWI) description contained in the work of *Gurnett et al.* [1995].

The Polar orbit has an ~86^0 inclination with an apogee of ~9 R_E and a perigee of ~1.8 R_E. The orbital period is about 18 hours. At

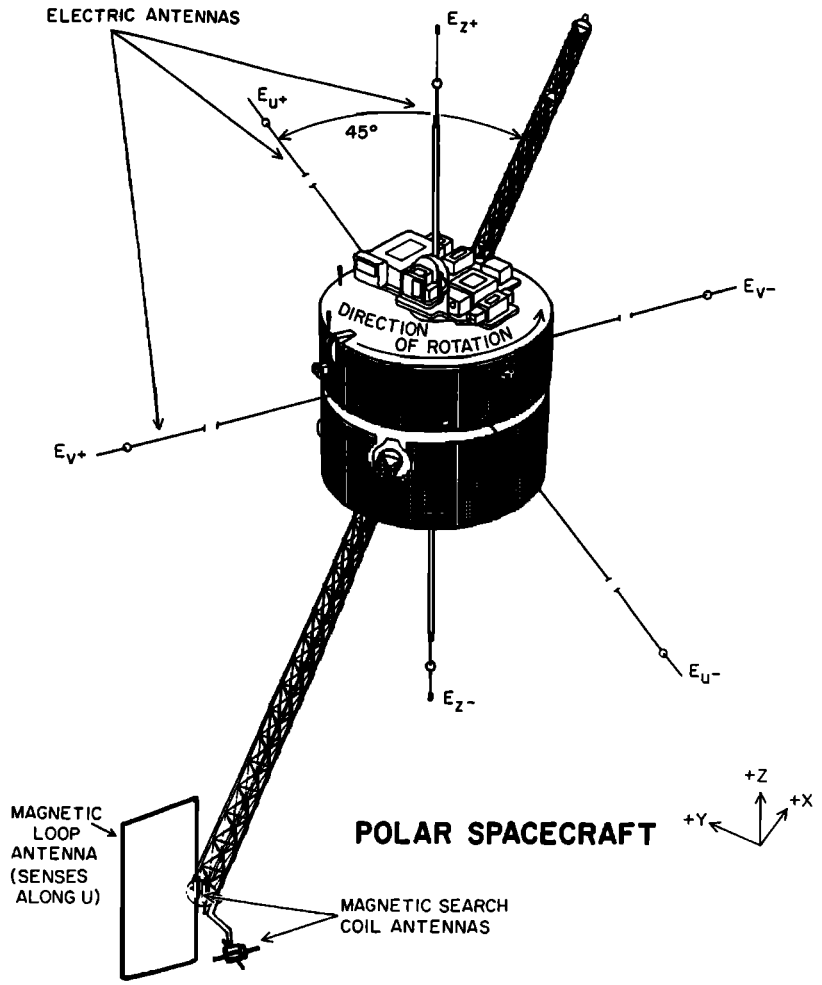

Figure 2. A schematic of the Polar spacecraft showing the orientation of the three orthogonal electric antennas (E_U, E_V and E_Z), the magnetic loop antenna (B_L), and the triaxial search coil antennas (B_U, B_V, and B_Z).

the beginning of the mission, the Polar apogee was set over the northern polar region. The location of the spacecraft is identified by orbital parameters (radial distance, magnetic local time and eccentric dipole L-shell value) obtained from Polar predictive and definitive obit data, and through the use of the Tsyganenko T89 model with Kp = 3-, 3, and 3+ options. At this stage of our analysis, the true geomagnetic activity has not been taken into account.

3. Results

Plate 1 is a frequency-time color spectrogram of the data obtained on April 7, 1996, from the Polar plasma wave multichannel analyzer while switched to the 130 m electric antenna located in the spin plane. This plot covers 24 hours as shown along the horizontal axis, and a frequency range of 5 Hz to 311 kHz, the MCA-E 's full frequency range, as shown along the vertical axis. The electric field power spectral density is plotted according to the color bar to the right of the spectrogram. The universal time (UT), radial distance from the center of the Earth (R_E), magnetic latitude (λ_M), magnetic local time (MLT), and approximate L - shell value, are indicated at the bottom of the plot.

On this day, Polar was first at its perigee around the south pole at 0140 UT, corresponding to a very high magnetic field strength and electron cyclotron frequency > 10^5 Hz. It next passed through the dayside plasmasphere/magnetosphere at ~ 0300 UT. Strong whistler mode waves (hiss and chorus) were detected in this latter region. At 0445 UT the spacecraft entered the northern hemisphere polar cap region by crossing the cusp and polar cap boundary layer. Inside the polar cap region some bursty waves are detected, but these are relatively weak. These polar cap wideband waves have an obvious upper cutoff frequency which corresponds to narrowband electron cyclotron emissions [*Gurnett and Frank*, 1978]. At the midpoint of the polar cap (orbit apogee), both the plasma frequency and electron cyclotron frequency reached their lowest values. Many auroral kilometric radiation (AKR) events can be noted inside the polar cap region at frequencies above 10^5 Hz. At 1450 UT, Polar moved from the polar cap to again cross a region of intense broadband waves, but on the nightside. The

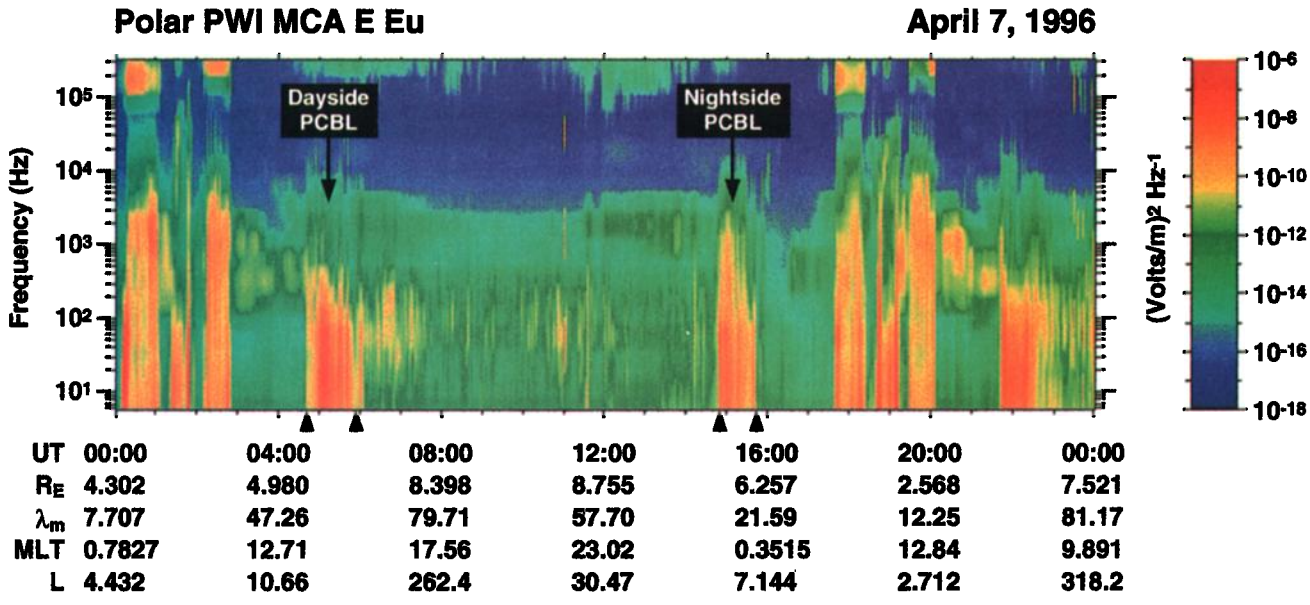

Plate 1. Color spectrogram of wave electric field from ~10^1 to 10^4 Hz and above. The boundary layer waves are indicated. In between the two boundary layer (dayside and nightside) crossings is the polar cap (quiet wave region).

spacecraft next entered the nightside plasmasphere and started another cycle. The waves seen at about 2130 UT are again the dayside PCBL waves. The waves seen from 0100-0200 UT and 1830-1930 UT are associated with the Polar spacecraft crossing the southern auroral zones and polar cap (it should be noted that the intense signals seen beginning at around 0000, 0200, 1730, and 1930 UT are not naturally occurring plasma waves but are rather a manifestation of antenna preamplifier oscillation as the spacecraft passes through the high density plasmasphere region). The various wave regions described above were identified by referring to orbit information, and plasma wave data. Wave properties have been examined to identify the general modes.

The wave intervals of interest are indicated by two sets of arrows along the time axis, and are designated as "Dayside PCBL" and "Nightside PCBL" within Plate 1. These intervals of intense waves bound magnetic fields that map into the polar cap region. Both wave events occur in the northern hemisphere near apogee. The dayside PCBL event occurs near 13.0 MLT and the other near 0.3 MLT, as the spacecraft orbit is in a near noon-midnight orientation.

The PCBL waves are characterized by bursts of "turbulence" covering a broad frequency range extending from f < 10^1 to 2 x 10^4 Hz as shown in the MCA electric field spectrum of Plate 1. The MCA best illustrates this nature of the waves since it has good temporal resolution. The magnetic field spectrum for these waves shows similar bursts. However, the intensity of the magnetic component of the waves is much nearer the background level of the receiver. Therefore the magnetic component is harder to discern in spectrogram format and is not presented here in that form. The region between the dayside PCBL and the nightside PCBL (about 0555 to 1450 UT) is identified as the northern polar cap. In this region there is typically a lack of strong signals although a few bursts of electrostatic noise are seen, as well as auroral hiss ($\lesssim$3 kHz) and auroral kilometric radiation ($\gtrsim$100 kHz). The vertical lines found at about 1100 UT are an instrument artifact caused by crosstalk from the SFR as it switched from logarithmic to linear mode.

Figure 3 shows the fractional amount of time that the waves are present from March 13 to August 31, 1996, on the dayside (0500 to 1800 UT) near Polar apogee. During this period the spacecraft apogee was in the northern hemisphere. For this statistical study, all passes were used except for those with data gaps. On some dawn-dusk orbits, there were two passes through the PCBL wave region. The total number of "crossings" for this interval was 254. Using the PWI SFR-A E_U plots, a wave "event" is marked by start and stop times identified by an observed increase in intensity (against background intensity) and a subsequent decrease. Our cutoff criterion was approximately 10^{-10} $(mV/m)^2$, determined by visual inspection of color spectral plots. The start and stop times were tabulated, as well as the spacecraft's location. For each hourly bin, the number of passes are indicated, as well as the number of times PCBL waves were detected. The plot shows that enhanced waves were present 100% of the time near local noon with a slightly lower occurrence rate at dawn and dusk. Preliminary analyses indicate that the wave intensities may be lower at dawn and dusk as well. The overall percentage of wave occurrence during this time interval was 96%.

The display of the geomagnetic latitude of the footpoint of the B - field line passing through the spacecraft versus geomagnetic local time for the events in Figure 3, are given in Figure 4a. In Figure 4a we use a magnetic local time resolution of 1 hour and a latitude resolution of 2°. For each northern hemisphere dayside pass and for each box the spacecraft passed through, we determine whether enhanced waves were present or not. The figure shows a general display of the location of where the waves are located. The waves map into a relatively narrowband of latitudes from 70° to 85°. This range gives the PCBL wave location. There is a trend for the PCBL waves to extend to slightly lower latitudes in both the dawn and dusk sides relative to the noon sector. Figure 4b shows the corresponding L values of the wave region versus geomagnetic local time. It is clear that PCBL waves observed on the dayside northern hemisphere occur predominantly in the region with $L \geq 10$. The wave location is slightly lower than cusp field lines (C. T. Russell, personal communication, 1997).

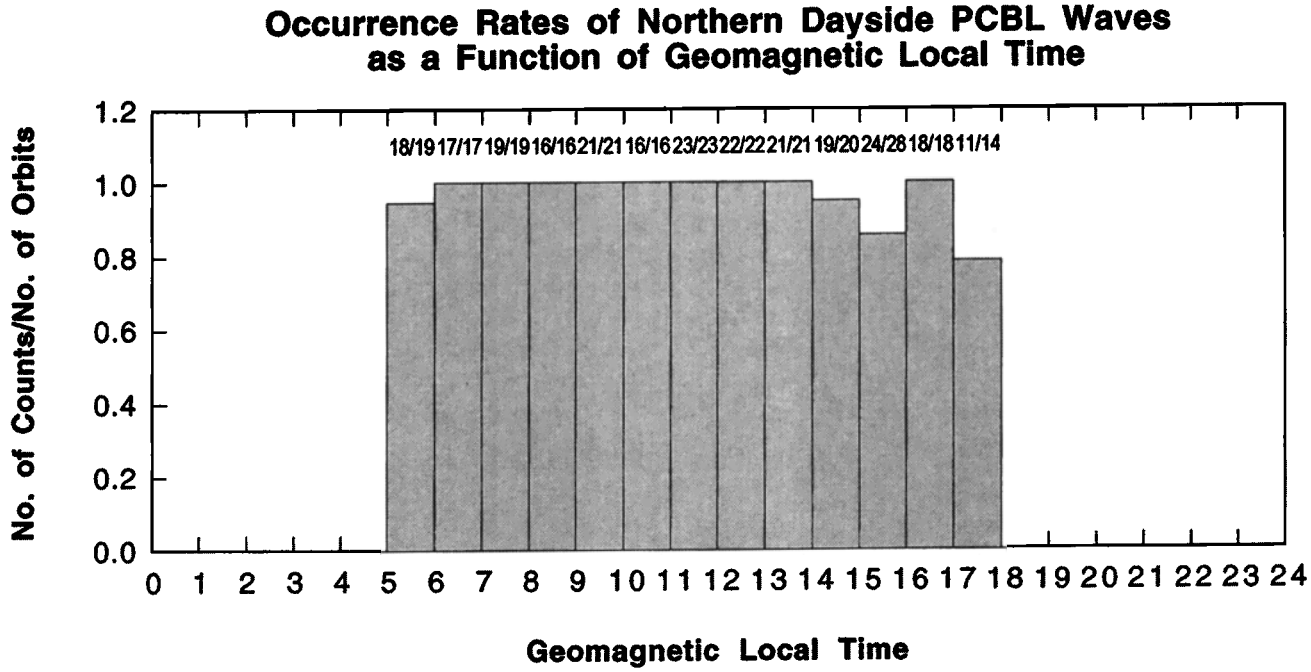

Figure 3. Occurrence frequency of northern dayside PCBL waves as a function of local time. The polar cap boundary layer waves are present on the dayside 96% of the time (0500-1800 LT). The statistics are listed at the top.

Wave power spectral densities have been studied for several PCBL events selected at random. Figures 5 and 6 show the electric and magnetic spectra of the two events occurring near the apogee in the northern hemisphere. A hand fit to the data has been drawn and the values for the fits are indicated in the graphs. The background (instrument) noise levels are also indicated for reference. The electron cyclotron frequency is indicated at the bottom of each figure. These latter values are calculated using the

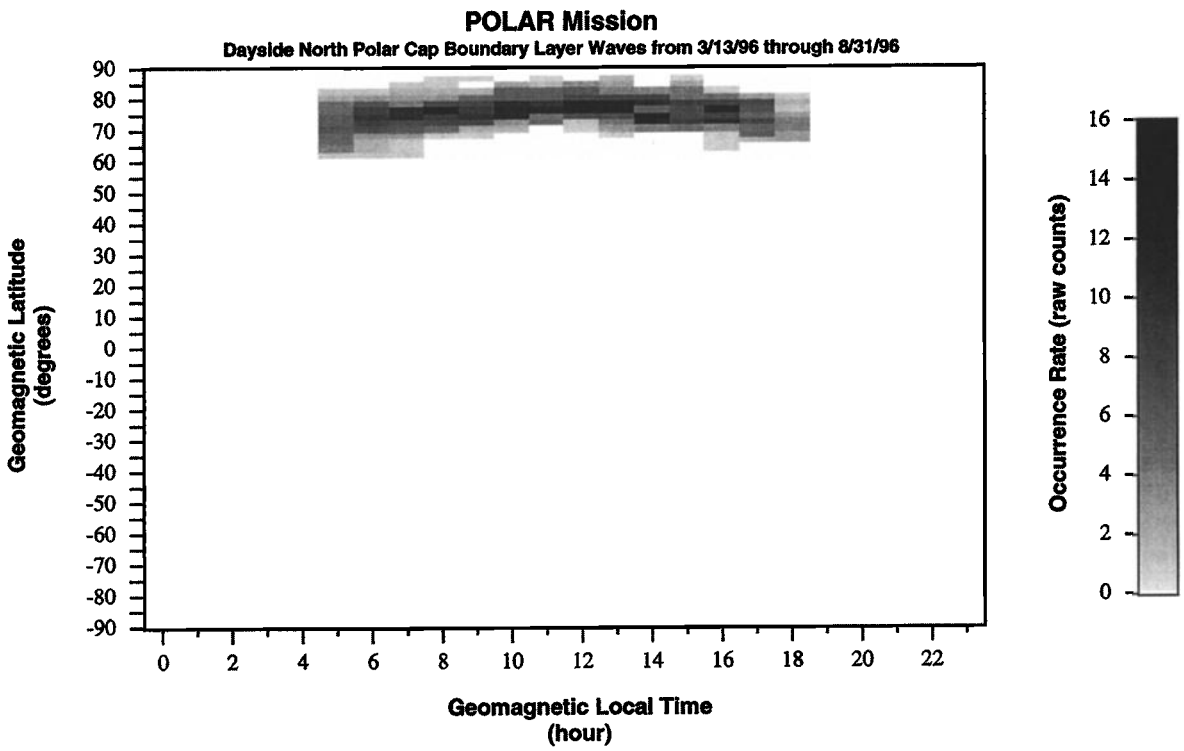

Figure 4a). The geomagnetic latitude of the foot point of the *B* field line passing through the spacecraft versus local time (GMT). Regions of wave activity are primarily located on the field lines whose footpoint geomagnetic latitudes lie between 70° and 80°. b) *L* - value distribution of the PCBL waves versus GMT. The wave region is located for L ≥ 10.

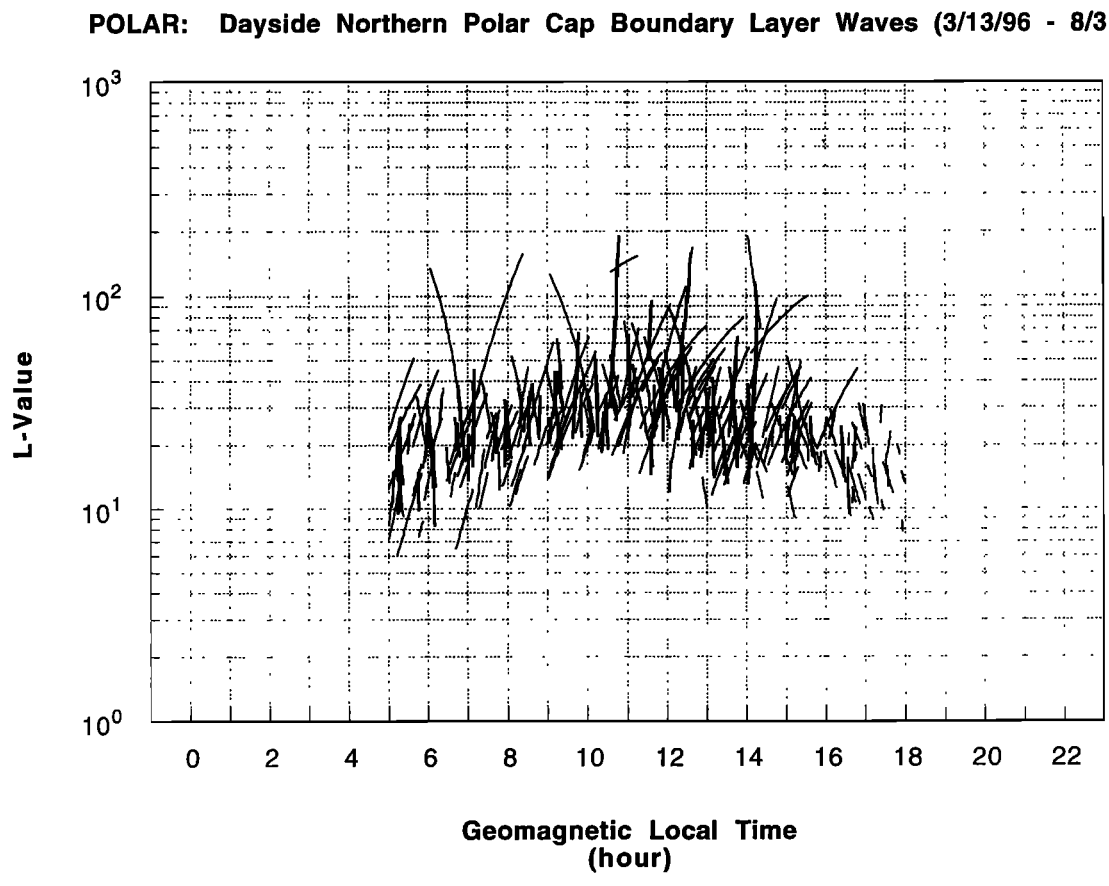

Figure 4. (continued)

onboard magnetometer data [*Russell et al.*, 1995]. The event shown in Figure 5 occurs on day 98, 1996 at 1302 MLT at 78.8° N invariant magnetic latitude. The wave frequency of the electric component extends to ~2 x 10^4 Hz (Figure 5a), and that of the wave magnetic component extends to ~ 3 x 10^3 Hz (Fig. 5b). The Figure 6 event occurs on day 114, 1996 at 1235 MLT at 76.3° N invariant latitude. The wave frequency for the electric component extends to ~10^4 Hz (Figure 6a) and that of the corresponding magnetic spectra extends to ~ 5 x 10^3 Hz (Figure 6b). Note that the electric component of the waves extends to frequencies above the electron cyclotron frequency. Although it appears that the wave magnetic component cuts off at the electron cyclotron frequency f_{ce} this is too close to the noise floor of the receiver to make any definite determination.

We have also examined the power spectra for the electric and magnetic components for the event near the Polar perigee in the southern hemisphere (not shown here). This event occurs on day 103, 1996 at 1353 MLT and invariant latitude 73.1°S. The frequencies of the electric spectrum extend to about 10^5 Hz and those of the magnetic spectrum to about 2 x 10^4 Hz. The wave intensities for this event are comparable to the two apogee events shown in Figures 5 and 6. This will be discussed later.

The spectral density plots for all the events discussed above have rough power - law shapes. The intensities and spectral shapes vary from event-to-event, but generally follow a power law. The E' waves clearly are present from ~10^1 Hz (the lowest frequency shown) to ~2 x 10^4 Hz for the apogee events. There are signals above this frequency but the results are less clear because the signal strength becomes close to the instrument noise level. The magnetic signals are broadbanded and appear to extend from ~10^1 Hz to the electron cyclotron frequency (6-7 x 10^3 Hz) with a fit of $f^{-2.7}$ in power spectra, on average.

High time resolution wideband receiver (WBR) data for the event occurring on day 114, 1996 are shown in Plate 2. In Plate 2 we have plotted 44 minutes from 0616 to 0700 UT on the horizontal axis versus frequency from 0 to 12 kHz on the vertical axis with color indicating the intensity of the signals. During this time, the WBR is switched to the electric E_u antenna and sampling data at the rate of 31.1 kHz. The data are formatted into a digital data stream and telemetered directly to a ground tracking station rather than tape recorded and telemetered to the ground at a much lower rate. Thus the WBR provides both good frequency resolution, assuming the appropriate bandpass filter has been chosen for the emission, and also excellent time resolution. In Plate 2 we note that the PCBL waves are very bursty. They last from tenths of seconds to tens of seconds, with the latter probably composed of several bursts occurring in succession or simultaneously. Around 0630 UT the waves extend up to 10 kHz, but the strongest part appears mainly below 4 kHz. The narrowband feature near 8 kHz appears to be the fundamental (n = 1) of the (n+1/2) f_{ce} electrostatic electron cyclotron harmonic (ECH) emission. The frequency of this narrow band electron cyclotron harmonic emission decreases with decreasing ambient magnetic field, falling from ~ 7 kHz at 0630 UT to ~ 6 kHz at

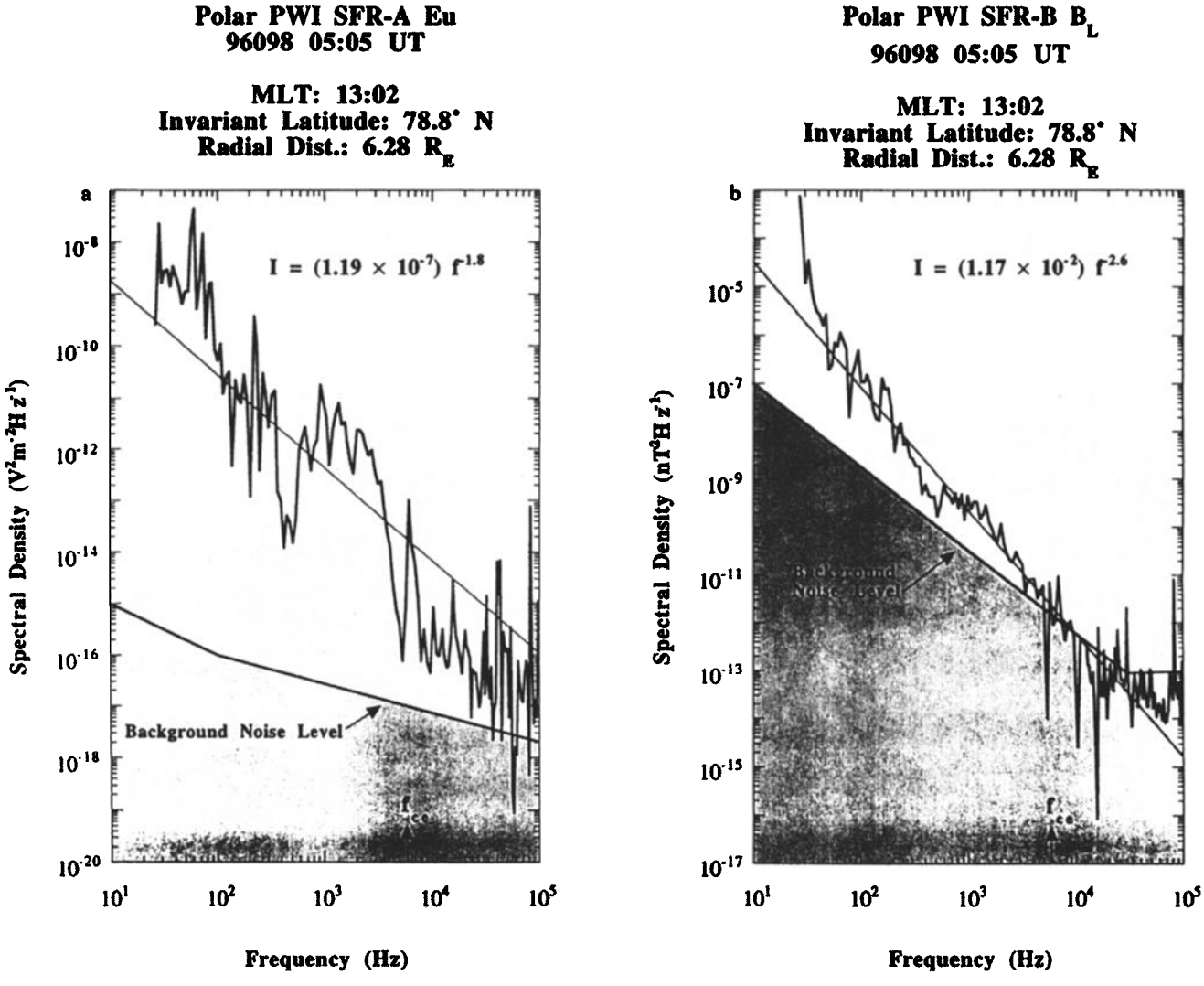

Figure 5. The (a) electric field and (b) magnetic field spectra for the events occurring on day 098, 1996. The background noise is indicated. The electric component of the waves extend beyond the electron cyclotron frequency (~6 x 10^3 Hz).

0700 UT. These overall results are generally consistent with the results from the other portion of the plasma wave instrument presented previously.

These broadband waves clearly have both a magnetic and an electric component. To try to identify the mode of propagation, we determine the B'/E' ratio for the events of Day 98 and 114, 1996, respectively for the two events shown in Figures 5 and 6. In Figures 7a and 7b we show the B'/E' ratio for the events of days 98 and 114, 1996, respectively.

The refractive index n for the obliquely propagating whistler waves in a cold uniform plasma for the case of $(2 f_{pe}^2 \cos\psi) >> (\sin^2\psi\, f\, f_{ce})$, and $f_{ce} \cos\psi > f$ (where f and f_{pe} are the wave frequency and the electron plasma frequency, respectively, and ψ is the angle of propagation with respect to the magnetic field direction) is given by

$$n = \frac{f_{pe}}{f^{1/2}(f_{ce}\cos\psi - f)^{1/2}} \quad (1)$$

In Figure 7 we have added two representative curves for the whistler refractive index for parallel propagation (ψ=0°) and for oblique propagation (at ψ=60°) as calculated from (1). The cold plasma density data used to derive the refractive indices were obtained from the Polar EFI experiment [*Harvey et al.*, 1995, F. S. Mozer, private communication, 1997]. Density values used are derived from a graph of measured spacecraft potential versus measured density that was collected from earlier spacecraft. The density values obtained in this manner fluctuated considerably during the wave events. For example, N_e values varied from 0.7 to 3.8 cm^{-3} for day 98 and 0.9 to 6 cm^{-3} for day 114. The above density values will thus have an uncertainty of approximately a factor of 2. We have used the maximum value of N_e in computing the whistler refractive indices. Since the electron plasma frequency is proportional to $(N_e)^{1/2}$ the B'/E' ratio may be high by ~40%. This is negligible compared to the orders of magnitude variations in the actual values.

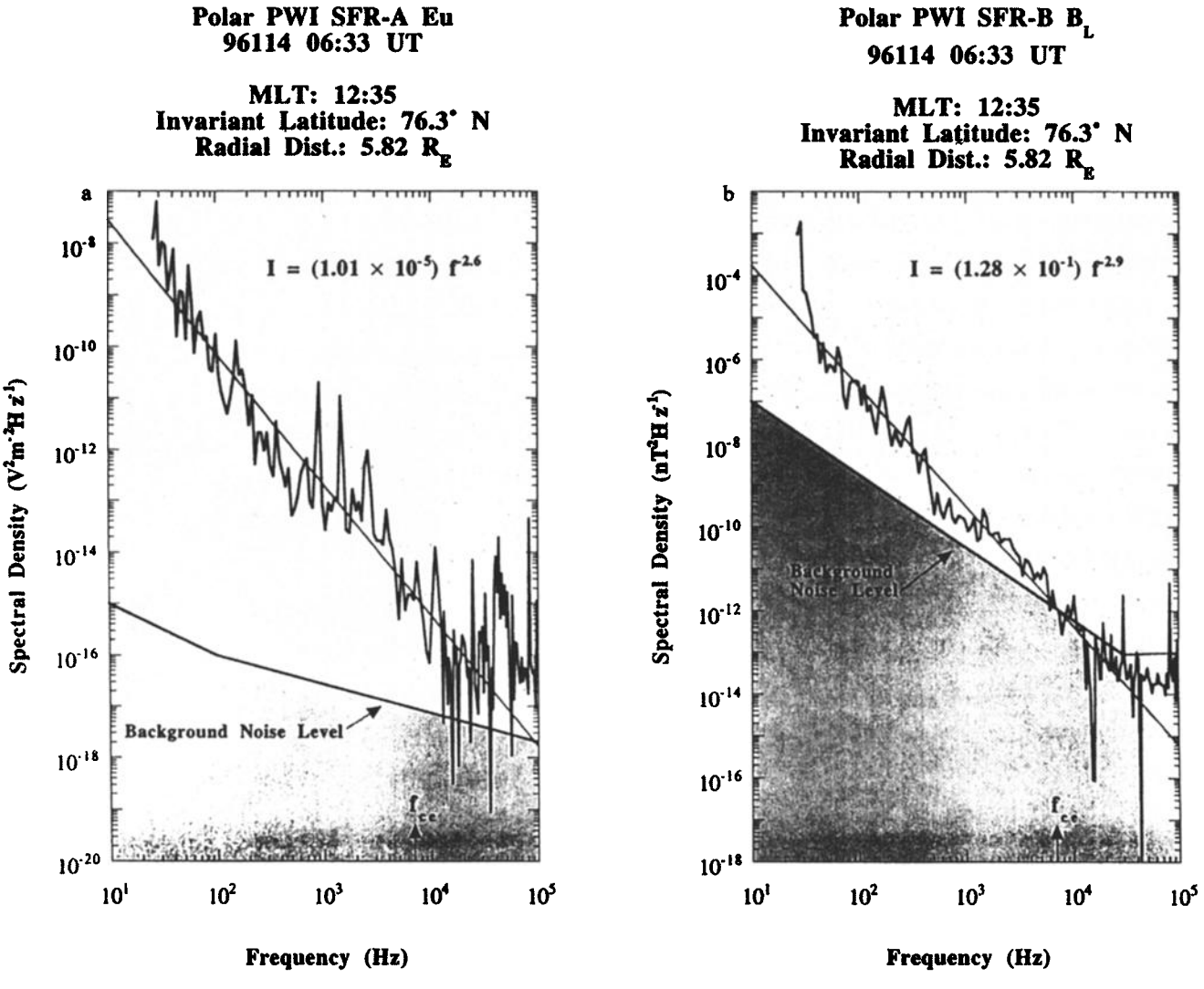

Figure 6. The (a) electric field and (b) magnetic field spectra for the event occurring on day 114, 1996. The sensor background noise is indicated. The electron cyclotron frequency is also noted. The electric component of the waves extend beyond the electron cyclotron frequency (~7 x 10^3 Hz).

For the two events, the B'/E' amplitude ratio generally fits the parallel propagating (ψ=0°) whistler wave curve at the lowest frequencies (f < 100 Hz). At mid (10^2 Hz < f < 10^3 Hz) and high (f > 10^3 Hz) frequencies, the B'/E' ratio shows considerable departure from the ψ=0° curve and a somewhat better fit with the ψ=60° curve. This clearly indicates that there could be considerable (off-axis) refraction associated with the higher frequency components. Strictly speaking, for oblique whistler wave propagation, n would correspond to B'/E'_T (where E'_T is the transverse electric field component with respect to the wave vector) rather than B'/E' ratio. It is possible that the PCBL region of enhanced plasma density acts as a wave guide and permits off-axis propagation with a minimum of wave damping. The B'/E' ratios lie in the range of 10 to 100. Thus the wave phase velocities range from 3 x 10^8 to 3 x 10^9 cm s^{-1}. These velocities are much higher than plasma convection speeds measured in this region of space, so Doppler shift effects on the phase velocities or on the B'/E' ratios should be negligible.

From Figure 1 we had noted that these PCBL waves occur on field lines that map into or close to the LLBL field lines. The wave characteristics presented here are also quite similar to those of the LLBL waves. In Table 1 we make an intercomparison between the Polar wave power spectra illustrated in this paper and the LLBL waves as measured by ISEE 1 and 2 and GEOS. We note that the GEOS event was much more intense than either ISEE 1 and 2 or Polar wave intensities. However, this event was somewhat anomalous because the spectra were taken during a magnetic storm when the magnetopause was pushed in to the spacecraft orbit (6.6 R_E). In addition, GEOS magnetic and electric sensors picked up the electromagnetic signals in the ultralow-frequency (~0-10 Hz) range. It is possible that the extraordinarily high solar wind ram pressure and intense southward interplanetary magnetic field B_z may have led to unusually high wave power during this event. Such LLBL wave intensity dependences on interplanetary parameters have been discussed at Earth and Jupiter by *Tsurutani et al.* [1989; 1997], respectively. Table 1 also lists a

spectrum for day 103, 1996 for Polar when it was near the southern hemisphere dayside perigee at ~2 R_E. We note that the wave intensities are of the same order as the high altitude northern hemispherical events.

Plates 3 and 4 show PWI broadband plasma waves and simultaneous ion fluxes (from the TIMAS experiment) for April 7 (day 98) and April 22 (day 113), 1996. The observed energetic ion populations have features typical of the midaltitude cusp [*Peterson*, 1985]. Prior to 0500 UT on April 7 and about 1240 UT on April 22, the energy and angular (not shown) distributions of the ions reveal primarily hot quasi-isotropic ion populations characteristic of the dayside magnetosphere. The energy-latitude(time) dispersion in the H^+ and He^{++} populations beginning about 0505 and 0530 UT on April 7 and about 1242 UT on April 22, are characteristic of the entry of magnetosheath plasma into the cusp or boundary layer. The regions of most intense wave activity (0500 to 0515 UT on April 7 and ~1240 to 1250 UT on April 22) are associated with significant changes in the angular distributions in the upflowing O^+ ions. Specifically, in these regions, the upflowing, relatively low-energy O^+ ions have angular distributions that are peaked at 50 to 70 degrees relative to the magnetic field direction. They have energies of a few hundred eV. The interpretation of H^+ angular distribution is rather complex as these intervals are characterized by down-going intense cusp H^+ fluxes having energy and angular distributions that overlap with the upcoming low-energy H^+ population. The TIMAS instrument was operated in a mode with limited angular resolution for He^+ ions during these intervals. We are not able to determine if the observed upflowing He^+ ion distribution is characterized by a conic angle larger or smaller than the one that characterizes the O^+ distributions.

The most probable mechanism for which the O^+ ions can gain significant energy transverse to the local magnetic field is through interactions with waves. Assuming that heating occurs primarily in the perpendicular direction, we can estimate the location of the region below the spacecraft. Because the magnetic field strength falls off roughly as r^{-3} and the first adiabatic invariant ($E_\perp/B$) is conserved (where $E_\perp$ is the perpendicular energy), we can estimate the maximum distance below the spacecraft where the transverse energy was possibly acquired. For conic angles of 50°, 60°, and 70° at an altitude typical for these observations (5.5 R_E), the maximum distances below the spacecraft where the transverse energy could be acquired are 0.9, 0.5, and 0.2 Earth Radii (R_E), respectively. These locations are quite close to the spacecraft, so the energization process is essentially a local one.

A systematic examination of the occurrence of these intense waves at the polar cap boundary at local times near dawn and dusk has shown that if upflowing O^+ ions are present at the time of these waves, the O^+ distribution has a characteristic conic angle indicating that significant transverse energy was acquired up to 1 R_E below the spacecraft. We note that there were intervals where intense waves were present, but no discernible upflowing O^+ ions were observed. The appearance of transversely energized O^+ ions simultaneous with enhanced wave intensity indicates that there is a strong possibility of near-local heating of the ions by the waves. However this is beyond the scope of the present paper, and another effort is in progress to address this issue.

4. Summary

Below are some of the main findings with regard to the PCBL waves:

1. The PCBL waves are present 96% of the time on the dayside (between 0500 and 1800 LT) at 6 to 8 R_E in the Polar orbit.

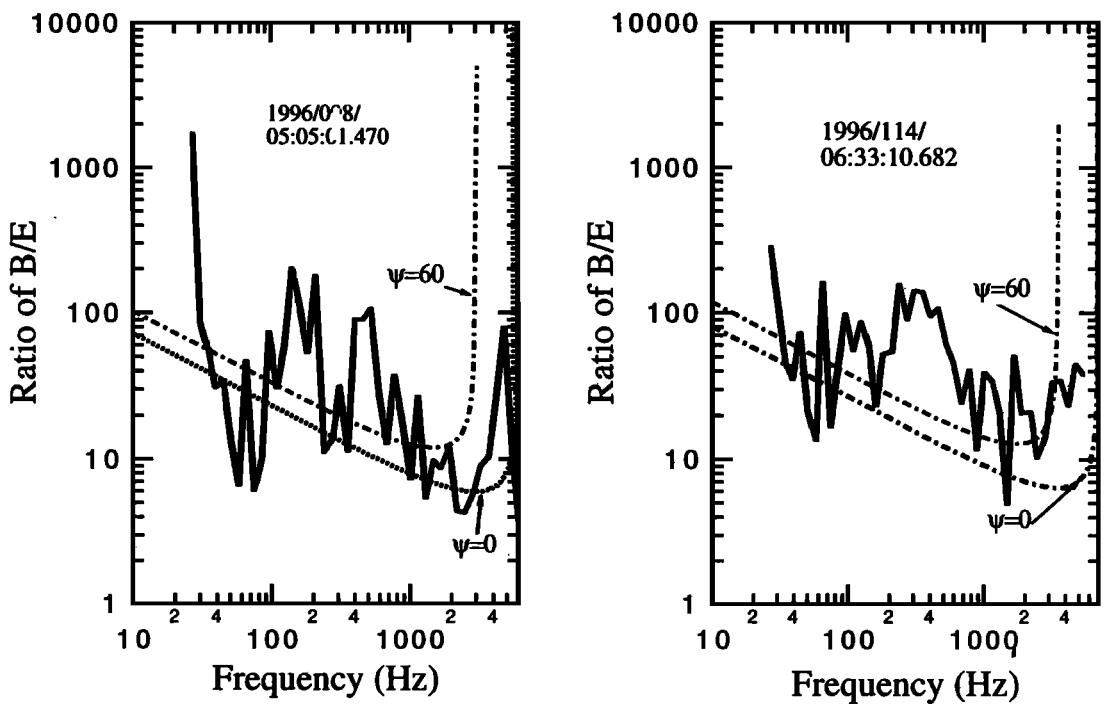

Figure 7. The B'/E' wave amplitude ratio for two events, one on day 98 and the other on day 114. Two curves corresponding to propagation angles of ψ=0° and ψ=60° for the whistler wave refractive index n are also shown. These ratios are highly variable but lie between the values 10 to 100. For parallel propagating whistler modes, the ratio B'/E' should lie along the ψ=0°curve.

2. The waves are located at 70° to 80° invariant magnetic latitude. This location is just below the cusp fields (75° to 85° latitude), (C.T. Russell, personal communication, 1997) and thus corresponds to LLBL field lines.
3. There is both an electric and a magnetic component to the waves. The electric component extends from ~10 Hz to 2 x 10^4 Hz and the magnetic from ~10 to 5 x 10^3 Hz.
4. The emissions are bursty, but when averaged over longer time intervals, they fit a rough power law with a $f^{-2.2}$ dependence for E' and $f^{-2.7}$ dependence for B' waves, on average.
5. The B'/E' ratio is consistent with the parallel propagating whistler mode waves for the low-frequency (10^1 - 10^2 Hz) component. However, the B'/E' ratio is often higher at mid (10^2 - 10^3 Hz) and high (10^3 to 6 x 10^3 Hz) frequencies, consistent with off-axis propagating waves.
6. The waves have very similar intensities, spectral shapes and E' and B' dependences as the LLBL waves. The PCBL waves are similar to the broadband noise on auroral field lines [*Gurnett and Frank*, 1977; *Gurnett et al.*, 1984], but unlike the latter, the PCBL waves do not have any clear peaks at any frequency.
7. The PCBL waves detected at low ~2 R_E altitudes are similar to those detected at high altitudes (6 to 8 R_E).
8. The intense noon sector wave events are well correlated with enhanced fluxes of 10 to 200 eV H^+, He^{++} and O^+ ions.

5. Discussion and Conclusion

Because the PCBL waves are quite similar to the LLBL waves, we assume that they are on the same magnetic field lines. A schematic of these field lines, the PCBL wave locations and the LLBL wave locations are shown in Figure 8. Although to date such waves have been identified at only three regions along the field lines (PCBL, LLBL and near Polar perigee), one can argue that the waves most likely exist along the entire length of the field lines. Here we have assumed that the field lines are "closed" and

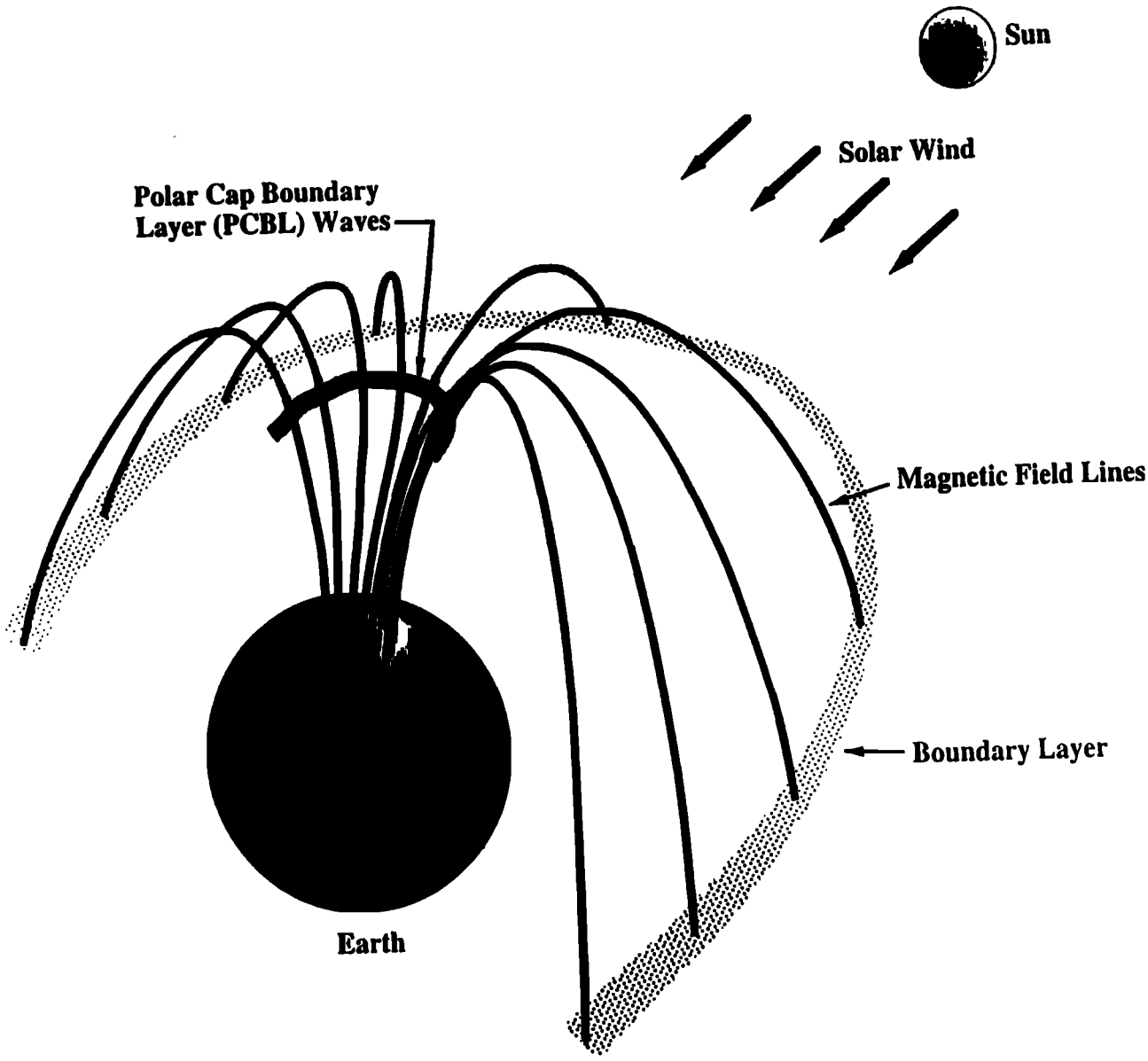

Figure 8. A northern polar view of the mapping of polar cap boundary layer (PCBL) waves to the low-latitude boundary layer (LLBL).

Table 1. A comparison of Polar broadband plasma wave properties and past observations from ISEE and GEOS

Spacecraft	Location	Date	B', $(nT)^2/Hz$	E', $(V/m)^2/Hz$
Polar (this paper)	~7-8 R_E altitude	day 098, 1996	$(1.17\times10^{-2})f^{-2.6}$	$(1.19\times10^{-7})f^{-1.8}$
	~2 R_E altitude	day 103, 1996	$(1.34\times10^{-2})f^{-2.5}$	$(1.22\times10^{-6})f^{-1.8}$
Ulysses *Tsurutani et al.* [1995]	Jupiter's magnetosphere	day 043, 1992	$(2.0\times10^{-4})f^{-2.4}$	$(4.0\times10^{-9})f^{-2.4}$
ISEE 1 *Gurnett et al.* [1979]	Earth's magnetopause	day 314, 1977	$\sim f^{-3.3}$	$\sim f^{-2.2}$
ISEE 1, 2 *Tsurutani et al.* [1981]	Earth's magnetopause	1977	$(1.0\times10^{1})f^{-3.9}$	$(3.0\times10^{-5})f^{-2.8}$
ISEE 1, 2 *Anderson et al.* [1982]	Earth's magnetopause	1977	$(7.90\times10^{-2})f^{-2.9}$	$(6.3\times10^{-6})f^{-2.2}$
GEOS 2 *Rezeau et al.* [1989]	Earth's magnetopause	day 240, 1978	$(3.60\times10^{1})f^{-2.6}$	$(1.20\times10^{-6})f^{-2.6}$
ISEE 1 *Tsurutani et al.* [1989]	Earth's magnetopause	1977-1978	$(3.00\times10^{-1})f^{-3.3}$	$(6.0\times10^{-7})f^{-2.1}$

The wave intensities and the spectral shapes are similar on Polar and ISEE. The reason for higher wave intensities on GEOS is discussed in the text.

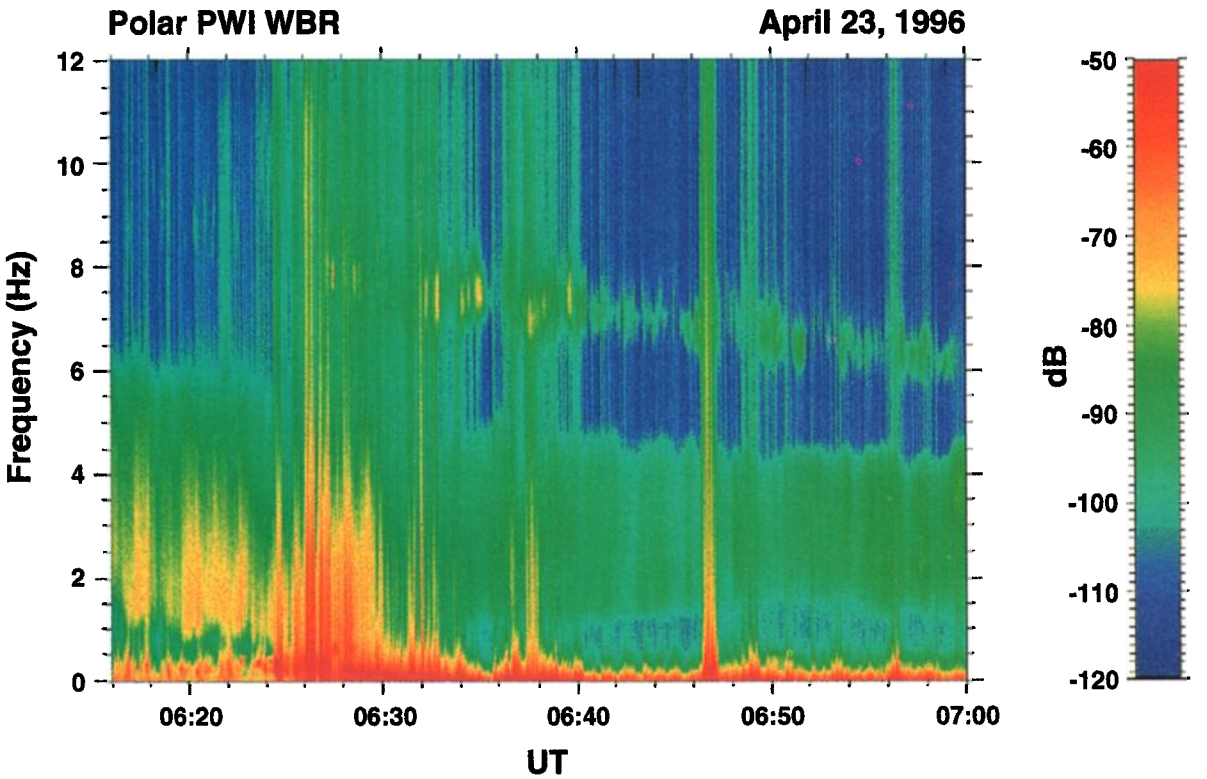

Plate 2. Wideband high time resolution plot for the PCBL wave event on Day 114, 1996. The waves are very spiky and highly variable in intensity.

extend from one hemispherical ionosphere to the other.

The PCBL wave field lines must be configured as indicated in Figure 8, where they map into the earth's ionosphere over a broad region of local times. Because the northern hemispherical waves are detected at only 6 to 8 R_E from the Earth on relatively strong fields, the chance they map into the cusp region is highly improbable. C. T. Russell (personal communication, 1997) has reported that the Polar magnetometer (statistically) detects cusp field lines at slightly higher latitudes and that the cusp only extends ±2 hours from local noon at Polar altitudes.

The three point intensity (LLBL, Polar near-apogee, Polar near-perigee) measurements give strong constraints on the wave source location. If wave generation occurs in the ionosphere, upward wave propagation would lead to wave intensity decreases (from Polar perigee to LLBL location) by orders of magnitude due to flux tube expansion alone. Wave damping and scattering would

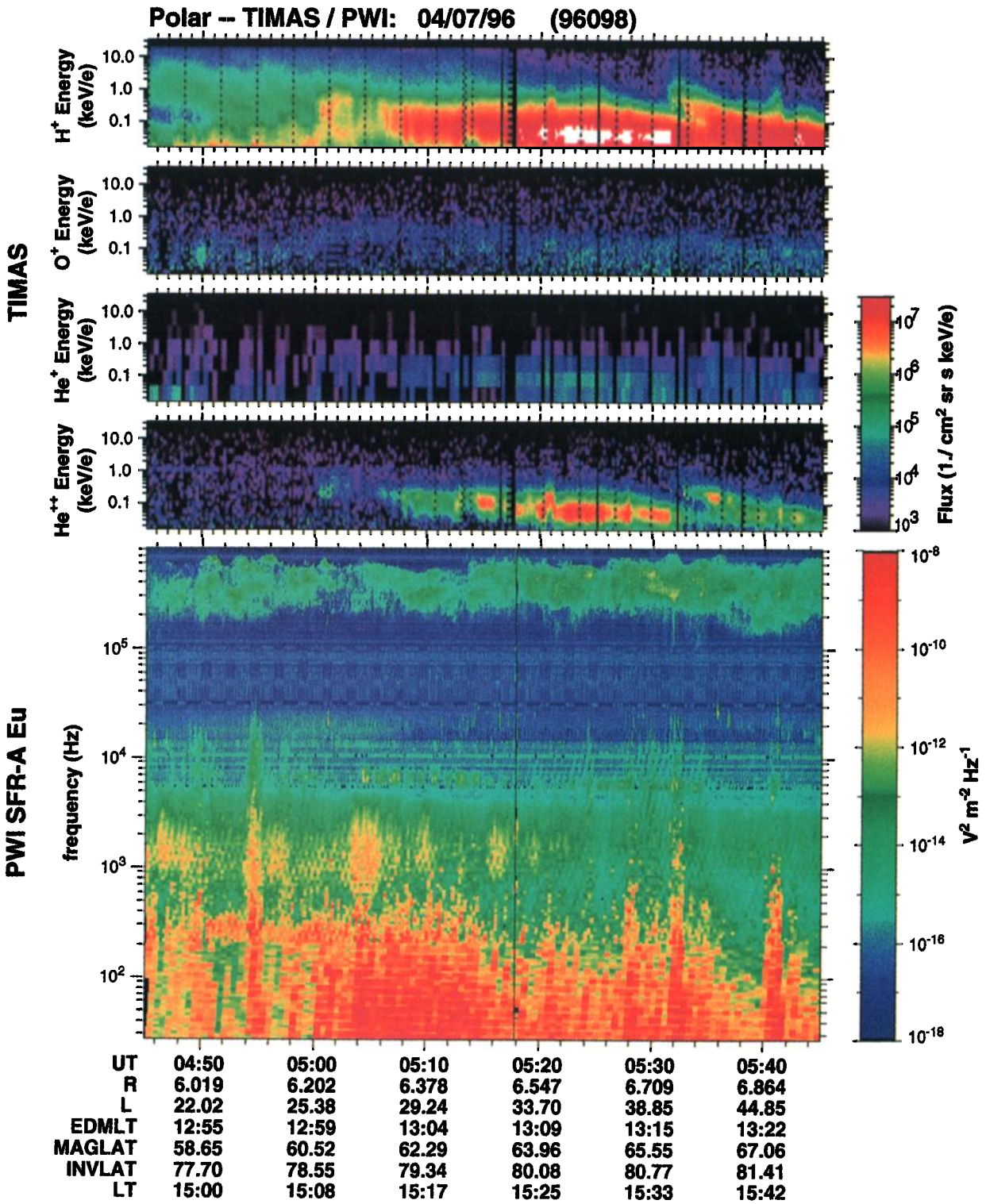

Plate 3. Color spectrogram of the H^+, O^+, He^+, and He^{++} ion fluxes observed by the TIMAS experiment (top 4 panels) and the electric component of the PWI broadband plasma wave event (lower panel) on day 98, 1996. The values of eccentric dipole magnetic local time (EDMLT), magnetic latitude (MAGLAT), invariant latitude (INVLAT) and local time (LT) are also shown at the bottom.

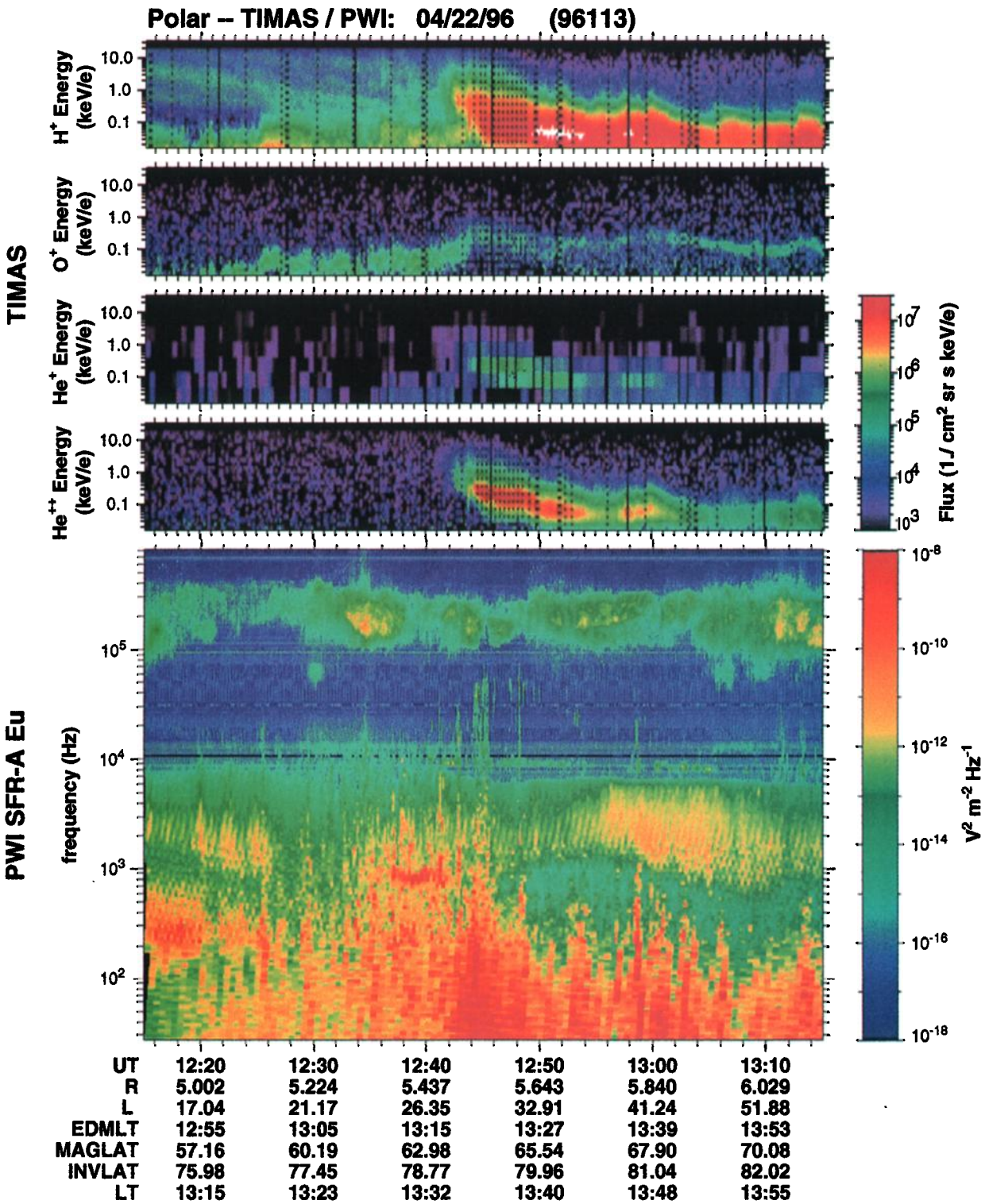

Plate 4. Color spectrogram of the ion fluxes and waves observed on day 113, 1996. The format is the same as in Plate 3.

decrease intensities further. Thus we can rule out an ionospheric source. Another possibility that has been discussed in the literature is that magnetosheath magnetosonic waves couple into LLBL Alfvén waves [*Johnson and* Cheng, 1997] or magnetosheath waves that are amplified at the magnetopause and propagate down the magnetic field lines [*Belmont et al.*, 1995]. If this were the case, then one would expect waves to be located primarily at noon with little or no waves present at the PCBL dawn and dusk flanks. There is some evidence for this (cf. Figure 3), however only slight. Moreover, this wave-coupling mechanism would work only for ultralow-frequency (ULF) waves which are much below the PCBL broadband plasma wave frequencies.

The most likely scenario is wave generation by a local source of free energy existing along field lines. Two possible sources are

Oxygen Ion Transport into the Plasmasheet During IMF B_s Events

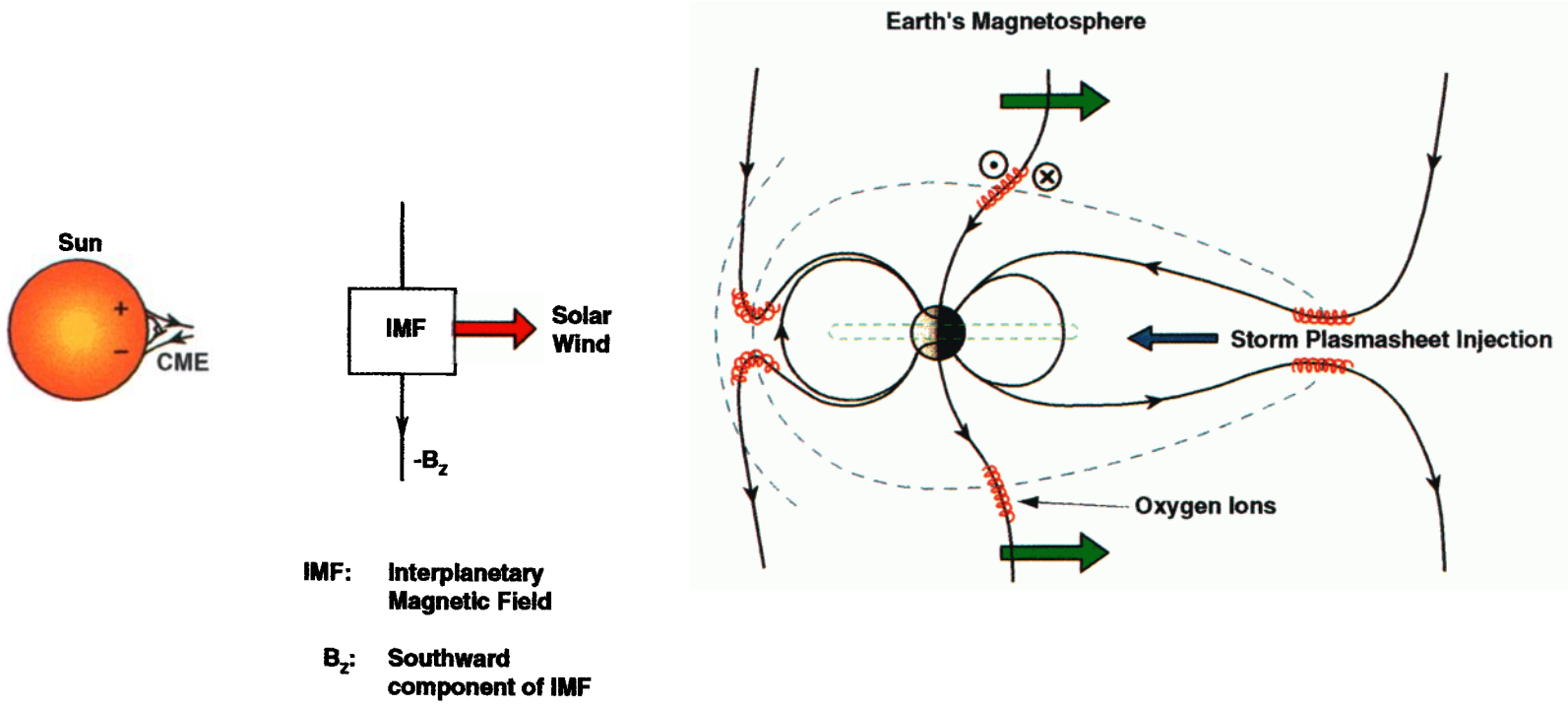

Plate 5. Oxygen ions heated in the PCBL/LLBL are convected into the plasmasheet during IMF B_s events. During magnetic storm periods, these ions will be injected into the nightside magnetosphere forming the storm-time ring current. Note that this mechanism has a natural delay from the storm main phase onset to the appearance of enhanced oxygen ions in the ring current.

field-aligned currents and density gradients. *Drake et al.* [1994a, b] have proposed current convective and whistler instabilities driven by the gradient of the field-aligned current as a possible mechanism for the generation of broadband plasma waves in the magnetopause current layer. Our preliminary theoretical analysis indicates that the presence of density gradients tends to stabilize both the current convective and whistler instabilities in the sense that their growth rates are reduced, and somewhat higher current gradients are needed to excite these modes [*Lakhina et al.*, 1997]. However, the density gradients introduce a finite real frequency to the current gradient driven modes. On the other hand, when the ions are hot, the lower hybrid drift instability can be excited provided the density gradients are sharp (approximately ion gyro radii) [*Gary and Eastman*, 1979; *Bhatia and Lakhina*, 1980; *Huba et al.*, 1981]. Weaker density gradients can excite drift modes [*Lakhina et al.*, 1993]. However, these modes correspond to ULF waves which occur at much lower frequencies than that of the PCBL broadband plasma waves discussed here.

The plasma and field results taken from this data set are currently being used to model instabilities of these types. In addition, hot plasma ray tracing models are being employed to examine the electromagnetic and electrostatic wave transport properties in this region of space. The density enhancements in the PCBL can act as "ducts" or wave guides for the waves. Also the plasma density gradient at the magnetopause, density gradients at the inner edge of the PCBL, and field curvature, will play strong roles in the wave propagation characteristics. Since the intense wave energy correlates with enhanced fluxes of energetic ions, interaction of these waves with the ions is expected to play an important role in the processes which lead to heating/acceleration of H^+, He^{++} and O^+ ions [*Chang and Coppi*, 1981; *Roy and Lakhina*, 1985; *Andre et al.*, 1990; *Crew et al.*, 1990; *Lakhina*, 1993; *Lakhina and Buti*, 1996]. The broadband plasma waves could precipitate energetic electrons and ions into the loss cone, leading to the excitation/enhancement of the auroral intensities.

One of the major puzzle for magnetic storm research is the origin of oxygen ions, which at times can dominate the energy density of the storm-time ring current (*Hamilton et al.*, 1988). The spectrum of the electric component of broadband plasma waves is roughly $f^{-2.2}$, as mentioned previously. For cyclotron damping of the electrostatic broadband waves, a $f^{-1.0}$ spectrum leads to equal energization for different mass ions (singly charged), and a steeper spectrum leads to greater energization for heavier (singly charged) particles. This is due to the greater wave power present at lower wave frequencies. This mechanism would provide for a preferential energization of O^+ over H^+, a feature commonly found in the ring current during intense magnetic storms. It is speculated that dayside boundary layer/cusp accelerated ions could be convected in the antisunward direction across the polar cap during IMF B_s events, to eventually populate the plasma sheet. Consequential injection of this plasma inward into the Earth's nightside magnetosphere could then naturally lead to enhanced oxygen ions in the ring current. A schematic illustrating this scenario is shown as Plate 5. This scenario would lead to a delay of oxygen ions appearance in the ring current, a feature that *Daglis* [1997] has noted in the double main phase storm event of March 24, 1991. However, we should mention that substorm electric fields can also produce ion beams and conics in the nightside auroral region, so this is another obvious potential source of plasmasheet ions. Further analyses are necessary to determine the contribution of each mechanism to the plasmasheet throughout the storm main phase and to a secondary main phase, if one should occur.

Acknowledgments: Portions of this paper represent work done at the Jet Propulsion Laboratory, and the California Institute of Technology, Pasadena, under contract with the National Aeronautics and Space Administration and under subcontract with the University of Iowa. J. S. Pickett and D. A. Gurnett acknowledge the support of NASA under NASA/GSFC contract NAS 5-30371. We thank C. T. Russell for providing Polar magnetic field data. Work at Lockheed Martin was supported by NASA contract NAS 5-33032. F. Mozer would like to acknowledge NASA contract NAS 5-30367 and grant NAS 5-3182 for support of portions of this effort. G. S. Lakhina would like to thank the National Research Council for the award of a Senior Resident Associateship at Jet Propulsion Laboratory.

The editor thanks two referees for their assistance in evaluating this paper.

References

Anderson, R.R., C.C. Harvey, M.M. Hoppe, B.T. Tsurutani, T.E. Eastman, and J. Etcheto, Plasma waves near the magnetopause, *J. Geophys. Res.*, *87*, 2087, 1982.

Andre, M., G.B. Crew, W.R. Peterson, A.M. Persoon, C.J. Pollock, and M.J. Engebretson, Ion heating by broadband low-frequency waves in the cusp/cleft, *J. Geophys. Res.*, *95*, 20809, 1990.

Axford, W.I., and C.O. Hines, A unifying theory of high-latitude geophysical phenomena and geomagnetic storms, *Can. J. Phys.*, *39*, 1433, 1961.

Belmont, G., F. Reberac, and L. Rezeau, Resonant amplification of magnetosheath MHD fluctuations at the magnetopause, *Geophys. Res. Lett.*, *22*, 295, 1995.

Bhatia, K.G., and G.S. Lakhina, Drift loss cone instability in the ring-current and plasmasheet, *Proc. Indian Acad. Sci. Earth Planet. Sci.*, *89*, 99, 1980.

Chang, T., and B. Coppi, Lower hybrid acceleration and ion evolution in the supra-auroral region, *Geophys. Res. Lett.*, *8*, 1253, 1981.

Crew, G.B., T. Chang, J.M. Retterer, W.K. Peterson, D.A. Gurnett, and R.H. Huff, Ion cyclotron resonance heated conics: Theory and observations, *J. Geophys. Res.*, *95*, 3950, 1990.

Daglis, I. A., The role of magnetosphere- ionosphere coupling in magnetic storm dynamics, in *Magnetic Storms*, *Geophys. Monogr. Ser.*, vol. *98*, edited by B. T. Tsurutani, W. D. Gonzalez, Y. Kamide, and J. K. Arballo, p. 107, Washington, D. C., 1997.

Drake, J. F., J. Gerber, and R. G. Kleva, Turbulence and transport in the magnetopause current layer, *J. Geophys. Res.*, *99*, 11211, 1994a.

Drake, J.F., R. G. Kleva, and M.E. Mandt, Structure of thin current layers: Implications for magnetic reconnection, *Phys. Rev. Lett.*, *73*, 1251, 1994b.

Drake, J. F., Magnetic reconnection, a kinetic treatment, in *Physics of the Magnetopause*, *Geophys. Monogr. Ser.*, vol. *90*, edited by P. Song et al., p. 155, AGU, Washington, D. C., 1995.

Gary, S.P., and T.E. Eastman, The lower hybrid drift instability at the magnetopause, *J. Geophys. Res.*, *84*, 7378, 1979.

Gendrin, R., Magnetic turbulence and diffusion processes in the magnetopause boundary layer, *Geophys. Res. Lett.*, *10*, 769, 1983.

Gurnett, D.A., and L.A. Frank, A region of intense plasma wave turbulence on auroral field lines, *J. Geophys. Res.*, *82*, 1031, 1977.

Gurnett, D. A. and L.A. Frank, Plasma waves in the polar cusp: Observations from Hawkeye, J. *Geophys. Res.*, *83*, 1447, 1978.

Gurnett, D.A., R.R. Anderson, B.T. Tsurutani, E.J. Smith, G. Paschmann, G. Haerendel, S.J. Bame, and C.T. Russell, Plasma wave instabilities at the magnetopause: Observations from ISEE 1 and 2, *J. Geophys. Res.*, *84*, 7043, 1979.

Gurnett, D.A., R.L. Huff, J.D. Menietti, J.L. Burch, J.D. Winningham, and S.D. Shawhan, Correlated low-frequency electric and magnetic noise along the auroral field lines, *J. Geophys. Res.*, *89*, 8971, 1984.

Gurnett, D.A., et al., The Polar plasma wave instrument, *Space Sci. Rev.*, *71*, 597, 1995.

Hamilton, D.C., G. Gloeckler, F.M. Ipavich, W. Stuedemann, B. Wilken, and G. Kremser, Ring current development during the great geomagnetic storm of February 1986, *J. Geophys. Res.*, *93*, 14343, 1988.

Harvey, P., et al., The electric field instrument on the Polar satellite, *Space Sci. Rev.*, *71*, 583, 1995.

Huba, J.D., N.T. Gladd, and J.F. Drake, On the role of the lower hybrid drift instability in substorm dynamics, *J. Geophys. Res.*, *86*, 5881, 1981.

Johnson, J. R., and C. Z. Cheng, Global structure of mirror modes in the magnetosheath, *J. Geophys. Res.*, *102*, 7179, 1997.

Kennel, C.F., and H.E. Petschek, Limit on stably trapped particle fluxes, *J. Geophys. Res., 71*, 1, 1966.

LaBelle, J., and R.A. Treumann, Plasma waves at the dayside magnetopause, *Space Sci. Rev., 47*, 175, 1988.

Lakhina, G.S., Low-frequency electrostatic noise due to velocity shear instabilities in the regions of magnetospheric flow boundaries, *J. Geophys. Res., 92*, 12161, 1987.

Lakhina, G.S., Generation of low-frequency electric field fluctuations on auroral field lines, *Ann. Geophys., 64*, 660, 1993.

Lakhina, G.S., and B. Buti, Stochastic acceleration by lower hybrid waves in solar corona, *Sol. Phys., 165*, 329, 1996.

Lakhina, G.S., P. K. Shukla, and L. Stenflo, Ultralow-frequency fluctuations at the magnetopause, *Geophys. Res. Lett., 20*, 2419, 1993.

Lakhina, G. S., B. T. Tsurutani, J. K. Arballo, C. M. Ho, and A. Boonsiriseth, Generation of broadband plasma waves in the polar cap boundary layer, *Eos, Trans. AGU, 78, Spring Meet. Suppl.*, S297, 1997.

Peterson, W. K., Ion injection and acceleration in the polar cap, in *The Polar Cusp*, edited by J. A. Holtet and A. Egeland, p. 63, D. Reidel, Norwell, Mass., 1985.

Pickett, J.S., et al., Correlative magnetopause boundary layer observations, *Eos, Trans. AGU, 78, Spring Meet. Suppl.*, S291, 1997.

Rezeau, L., A. Morane, S. Perraut, A. Roux, and R. Schmidt, Characterization of Alfvénic fluctuations in the magnetopause boundary layer, *J. Geophys. Res., 94*, 101, 1989.

Roy, M., and G.S. Lakhina, Lower hybrid wave model for aurora, *Astrophys. Space Sci., 117*, 111, 1985.

Russell, C.T., R.C. Snare, J.D. Means, D. Pierce, D. Dearborn, M. Larson, G. Barr and G. Le, The GGS/Polar magnetic fields investigation, *Space Sci. Rev., 71*, 563, 1995.

Shelley, E.G., et al., The toroidal imaging mass-angle spectrograph (TIMAS) for the Polar mission, *Space Sci. Rev., 71*, 497, 1995.

Tsurutani, B.T., and W.D. Gonzalez, The efficiency of "viscous interaction" between the solar wind and the magnetosphere during intense northward IMF events, *Geophys. Res. Lett., 22*, 663, 1995.

Tsurutani, B.T., and R.M. Thorne, Diffusion processes in the magnetopause boundary layer, *Geophys. Res. Lett., 9*, 1247, 1982.

Tsurutani, B.T., E.J. Smith, R.M. Thorne, R.R. Anderson, D.A. Gurnett, G.K. Parks, C.S. Lin, and C.T. Russell, Wave-particle interaction at the magnetopause: Contribution to the dayside aurora, *Geophys. Res. Lett., 8*, 183, 1981.

Tsurutani, B.T., A.L. Brinca, E.J. Smith, T. Okada, R.R. Anderson, and T.E. Eastman, A survey of ELF-VLF plasma waves at the magnetopause, *J. Geophys. Res., 94*, 1270, 1989.

Tsurutani, B.T., D. J. Southwood, E.J. Smith, and A. Balogh, A survey of low-frequency waves at Jupiter: The Ulysses encounter, *J. Geophys. Res., 98*, 21, 203, 1993.

Tsurutani, B.T., et al., Plasma wave characteristics of the Jovian magnetopause boundary layer: Relationship to the Jovian aurora?, *J. Geophys. Res., 102*, 4751, 1997.

Zhu, Z., P. Song, J.F. Drake, C.T. Russell, R.R. Anderson, D.A. Gurnett, K.W. Ogilvie, and R.J. Fitzenreiter, The relationship between ELF-VLF waves and magnetic shear at the dayside magnetopause, *Geophys. Res., Lett., 23*, 773, 1996.

J. K. Arballo, A. Boonsiriseth, C. Galvan, C. M. Ho, G. S. Lakhina and B. T. Tsurutani, Jet Propulsion Laboratory, California Institute of Technology, MS 169-506, 4800 Oak Grove, Drive, Pasadena, CA 91109. (email: jarballo@jplsp.jpl.nasa.gov; cho@jplsp.jpl.nasa.gov; lakhina@jplsp.jpl.nasa.gov; btsurutani@jplsp.jpl.nasa.gov).

D. A. Gurnett and J. S. Pickett, Department of Physics and Astronomy, The University of Iowa, Iowa City, IA 52242.

W. K. Peterson, Lockheed Space Science Laboratory, Palo Alto, CA 94304.

R. M. Thorne, Department of Atmospheric Science, University of California Los Angeles, Los Angeles, CA 90024.

(Received March 21, 1997; revised October 20, 1997;
accepted October 21, 1997.)